Assessment of Global and Regional Lung Compliance in Pulmonary Fibrosis With Hyperpolarized Gas MRI

Ming Zhang, PhD,[1,2] Haidong Li, PhD,[1,2] Yi Xiao, MD,[3] Hongchuang Li, BS,[1,2] Xiaoling Liu, BS,[1,2] Xiuchao Zhao, PhD,[1,2] Yu Zheng, BS,[1,2] Yeqing Han, MS,[1,2] Fumin Guo, PhD,[1] Xianping Sun, BS,[1,2] Jianping Zhao, MD,[4] Shiyuan Liu, MD,[3*] and Xin Zhou, PhD[1,2,5*]

Background: Lung compliance, a biomarker of pulmonary fibrosis, is generally measured globally. Hyperpolarized ^{129}Xe gas MRI offers the potential to evaluate lung compliance regionally, allowing for visualization of changes in lung compliance associated with fibrosis.
Purpose: To assess global and regional lung compliance in a rat model of pulmonary fibrosis using hyperpolarized ^{129}Xe gas MRI.
Study Type: Prospective.
Animal Model: Twenty Sprague–Dawley male rats with bleomycin-induced fibrosis model (N = 10) and saline-treated controls (N = 10).
Field Strength/Sequence: 7-T, fast low-angle shot (FLASH) sequence.
Assessment: Lung compliance was determined by fitting lung volumes derived from segmented ^{129}Xe MRI with an iterative selection method, to corresponding airway pressures. Similarly, lung compliance was obtained with computed tomography for cross-validation. Direction-dependencies of lung compliance were characterized by regional lung compliance ratios (R) in different directions. Pulmonary function tests (PFTs) and histological analysis were used to validate the pulmonary fibrosis model and assess its correlation with ^{129}Xe lung compliance.
Statistical Tests: Shapiro–Wilk tests, unpaired and paired *t*-tests, Mann–Whitney *U* and Wilcoxon signed-rank tests, and Pearson correlation coefficients. $P < 0.05$ was considered statistically significant.
Results: For the entire lung, the global and regional lung compliance measured with ^{129}Xe gas MRI showed significant differences between the groups, and correlated with the global lung compliance measured using PFTs (global: $r = 0.891$; regional: $r = 0.873$). Additionally, for the control group, significant difference was found in mean regional compliance between areas, eg, 0.37 (0.32, 0.39) $\times 10^{-4}$ mL/cm H_2O and 0.47 (0.41, 0.56) $\times 10^{-4}$ mL/cm H_2O for apical and basal lung, respectively. The apical-basal direction R was 1.12 ± 0.09 and 1.35 ± 0.13 for fibrosis and control groups, respectively, indicating a significant difference.
Data Conclusion: Our findings demonstrate the feasibility of using hyperpolarized gas MRI to assess regional lung compliance.
Evidence Level: 2
Technical Efficacy: Stage 1

J. MAGN. RESON. IMAGING 2024.

View this article online at wileyonlinelibrary.com. DOI: 10.1002/jmri.29497

Received Mar 11, 2024, Accepted for publication Jun 6, 2024.

*Address reprint requests to: X.Z., 30 West Xiaohongshan, Wuhan 430071, China. E-mail: xinzhou@wipm.ac.cn, or S.L., No. 415 Fengyang Road, Shanghai 200003, China. E-mail: cjr.liushiyuan@vip.163.com
Ming Zhang, Haidong Li, and Yi Xiao contributed equally to this work.

From the [1]Key Laboratory of Magnetic Resonance in Biological Systems, State Key Laboratory of Magnetic Resonance and Atomic and Molecular Physics, National Center for Magnetic Resonance in Wuhan, Wuhan Institute of Physics and Mathematics, Innovation Academy for Precision Measurement Science and Technology, Chinese Academy of Sciences-Wuhan National Laboratory for Optoelectronics, Huazhong University of Science and Technology, Wuhan, China; [2]University of Chinese Academy of Sciences, Beijing, China; [3]Department of Radiology, Changzheng Hospital of the Second Military Medical University, Shanghai, China; [4]Department of Respiratory and Critical Care Medicine, Tongji Hospital, Tongji Medical College, Huazhong University of Science and Technology, Wuhan, China; and [5]School of Biomedical Engineering, Hainan University, Haikou, China

Additional supporting information may be found in the online version of this article

Pulmonary fibrosis is a chronic lung disease characterized by the excessive accumulation of extracellular matrix and remodeling of the lung architecture.[1] Idiopathic pulmonary fibrosis (IPF) represents the most severe and prevalent form, often leading to a dismal prognosis with a median survival period of 2 to 3 years post-diagnosis of IPF.[2] Lung compliance, defined as the change in lung volume per unit change in transmural pressure gradient, serves as an indicator of the lung's capacity for expansion and contraction.[3] This parameter has been observed to decrease early in pulmonary fibrosis, and its reduction correlates with disease progression.[3] This may be attributed to the thickened and stiffened pulmonary tissue, which hinders lung inflation.

Lung compliance is commonly measured using a ventilator and esophageal balloon in clinical routine.[4] However, this technique only provides global measurement of lung compliance, making it difficult to investigate regional complications of highly heterogeneous lung diseases such as IPF. This limitation can hinder accurate characterization of lung disease and patient management. Pulmonary imaging provides a way to quantify lung compliance regionally, offering valuable insights into understanding IPF mechanisms and facilitating the development of new treatments.[5] For example, multi breath-hold computed tomography (CT) has been reported for regional static lung compliance assessment.[6] Additionally, four-dimensional thoracic CT ventilation imaging has been used to quantify regional dynamic lung compliance within multiple scans.[5] However, the ionizing radiation burden limits the routine clinical use of CT. Electrical impedance tomography offers an alternative for local lung compliance assessment by measuring the regional lung volume changes via measuring the changes in impedance in lung tissues.[7] However, the inherently poor spatial resolution represents a substantial limitation.[8] Importantly, these techniques could only indirectly evaluate local lung compliance because they are unable to directly measure gas volume in the lung.[7,9] Imaging methods that facilitate direct gas volume measurement are crucial for the precise evaluation of regional lung compliance, serving as the foundation for clinical applications.

Hyperpolarized ^{129}Xe gas MRI has emerged as a potent tool for regional pulmonary anatomical and functional evaluation, given its ability to directly visualize xenon gases in the lung.[10–13] This may allow for an accurate depiction of inhaled gas distribution within the alveoli and distal airways. Furthermore, lung inflation can be assessed by administering varying volumes of xenon gases.[14] Previous studies have suggested that ^{129}Xe MRI can precisely measure lung airspace volume with good sensitivity and reproducibility.[15,16] A prior study used hyperpolarized ^{129}Xe MRI acquired at two pressure points to quantify the global lung compliance in healthy animals.[17] While previous studies indicated potential for global rather than regional measurement of lung compliance, the feasibility for regional lung compliance measurement in characterizing lung disease remains unexplored.[17,18] Furthermore, previous study has shown functional gravitational gradients in lung gas exchange.[13] Whether lung compliance exhibits similar characteristics, like direction-dependencies, remains unknown. This parameter may help reveal in which direction the lungs are more prone to expansion and dilation.

Against this background, we aimed to assess global and regional lung compliance measurements with ^{129}Xe MRI in comparison to pulmonary function tests (PFTs). Furthermore, we aimed to quantify and compare direction-dependencies of regional lung compliance between a control and fibrosis group.

Materials and Methods

All animal experimental protocols were approved by the Institutional Review Board and performed according to the national Regulations for the Administration of Affairs Concerning Experimental Animals.

Animal Preparation

Twenty male Sprague–Dawley rats (mean weight 200 ± 20 g, Hubei Provincial Center for Disease Control and Prevention, Wuhan, Hubei, China) were randomly divided into two groups (N = 10 each) after acclimatization. The fibrosis group received a 0.4 mL solution of bleomycin (2.5 U/kg body weight; Shanghai Yuanye Bio-Technology, Shanghai, China) via intratracheal instillation, and the control group received an equivalent amount of normal saline.[19] Prior to surgery, rats were induced anesthesia with 5% isoflurane (RWD, Shenzhen, Guangdong, China), and were maintained with 2% isoflurane during the surgery. PFTs, ^{129}Xe gas MRI, CT, and histology analysis were conducted sequentially on one rat before moving on to the next. All the measurements were performed between day 21 and day 23 after treatment.[20] During the experiments, all the rats were 9 weeks old, and the weight was 269 ± 12 g for the control group and 253 ± 29 g for the fibrosis group.

Pulmonary Function Tests

The PFTs were performed for each rat using a Forced Maneuvers system (CRFM 100; EMMS, Alton, Hants, UK). Before the experiments, the rats were anesthetized with sodium pentobarbital (30 mg/kg, intraperitoneal injection, PlantChemMed, Shanghai, China) and then intubated with 14-G endotracheal tubes. Within 5 minutes, inspiratory capacity (IC), forced vital capacity (FVC), quasi-static lung compliance (C_{qs}), and total lung capacity (TLC) were obtained.[21]

Hyperpolarized ^{129}Xe MRI Experiments

After PFTs, all rats were imaged using a 7-T animal MRI scanner (Bruker Biospec 70/20 USR, Billerica, MA, USA) equipped with a home-built dual-tuned birdcage coil. The rats were anaesthetized with 2% isoflurane and maintained throughout the imaging procedure. Animals were placed in supine position in the scanner and alternately ventilated with hyperpolarized ^{129}Xe (approximately 40% polarization, verImagin Healthcare, Wuhan, Hubei, China) or oxygen gas using a home-built MRI-compatible gas delivery system,[21,22]

which can record the airway pressure in real time and trigger MRI acquisition by using a logic voltage level.

For ^{129}Xe MRI, as shown in Fig. 1, each rat was flushed with xenon gases three times to minimize the influence of longitudinal relaxation (T_1) decay on lung volume measurements (Fig. S1 in the Supplemental Material). Then, a fast low-angle shot (FLASH) sequence was applied during the following breath-hold, with the following parameters: repetition time (TR)/echo time (TE) = 7.4 msec/2.7 msec, flip angle = 12°, centric encoding, number of slices = 24, slice thickness = 1.6 mm, field of view (FOV) = 50 mm × 50 mm, matrix = 64 × 64, and the voxel size = 0.98 mm^3. To obtain ^{129}Xe MRI data at different airway pressures, the rats were administered with different volumes of xenon gases (flow rate: 0.4 mL/100 msec) by adjusting the inhalation time after the third end expiration (initial inhalation time is 100 msec, with an increment of 100 msec), and xenon images were acquired under breath-hold conditions. The number of ^{129}Xe images was determined by the maximum breath-hold pressure of 10 cm H_2O, and typically six to nine images were acquired from each rat. The rats were ventilated with oxygen 15 times between two consecutive ^{129}Xe image acquisitions.

Chest CT Experiments

After MRI examinations, chest CT scans were also acquired on each rat using a CT scanner (uCT 780; United Imaging, Shanghai, China). During the imaging examination, the rat was positioned supine and ventilated with oxygen gas using a home-built ventilator, and 2% isoflurane was used for maintaining anesthesia. Similar to the ventilation strategy used in ^{129}Xe MRI examinations, the volume of oxygen gas ventilated to the rat was also controlled by the inhalation time (started from 100 msec with a step of 100 msec). The airway pressures were recorded throughout the experiment, and CT images were acquired within 3 seconds during breath-hold phases. All CT images were acquired with the following parameters: tube voltage = 120 kV, FOV = 60 mm × 60 mm, and the reconstructed spatial resolution = 0.23 × 0.23 × 0.23 mm^3, resulting in a voxel size of 0.01 mm^3. The images of one rat in the control group were excluded from the subsequent analysis due to the failure to record airway pressure.

Global and Regional Lung Compliance Calculation

The ^{129}Xe ventilation images were reconstructed using Matlab software (version 2021a; The MathWorks Inc., Natick, MA, USA). Ventilation areas were segmented using an iterative selection method after removing the large airways manually for calculating lung volumes.[23] Global static lung compliance measured with hyperpolarized ^{129}Xe MRI (C_{Xe}) was calculated by linearly fitting using the following equation:

$$\Delta V_{Xe}(i) = C_{Xe} \cdot \Delta P_{Xe}(i), i = 1, \ldots, n, \quad (1)$$

$$\Delta V_{Xe}(i) = V_{Xe}(i) - V_{Xe}(0); \Delta P_{Xe}(i) = P_{Xe}(i) - P_{Xe}(0),$$

where $V_{Xe}(i)$ and $V_{Xe}(0)$ are the total lung volume measured using the segmented ^{129}Xe ventilation images under the airway pressure $P_{Xe}(i)$ and $P_{Xe}(0)$, respectively, with $i = 1 \ldots n$, and n represents the number of pressure points.

Three-dimensional (3D) regional lung compliance measured with hyperpolarized ^{129}Xe MRI (C_{Xe_map}) was also calculated (Fig. 1). For each rat, ^{129}Xe ventilation images acquired under different airway pressures of $P_{Xe}(1)$, …, $P_{Xe}(n)$ were registered to the image with minimal pressure ($P_{Xe}(0)$, inhalation time of 100 msec) using Advanced Normalization Toolkits (version:2.2.0; https://github.com/stnava/ANTs/) as described in previous study.[24,25] The resulting deformation field $\Psi_{Xe\text{-}P(i)}, i = 1 \ldots n$, was used to calculate the Jacobian determinant maps $J(\Psi_{Xe\text{-}P(i)})$ that describe the volume scaling factor. The volume maps with different pressures were calculated as follows:

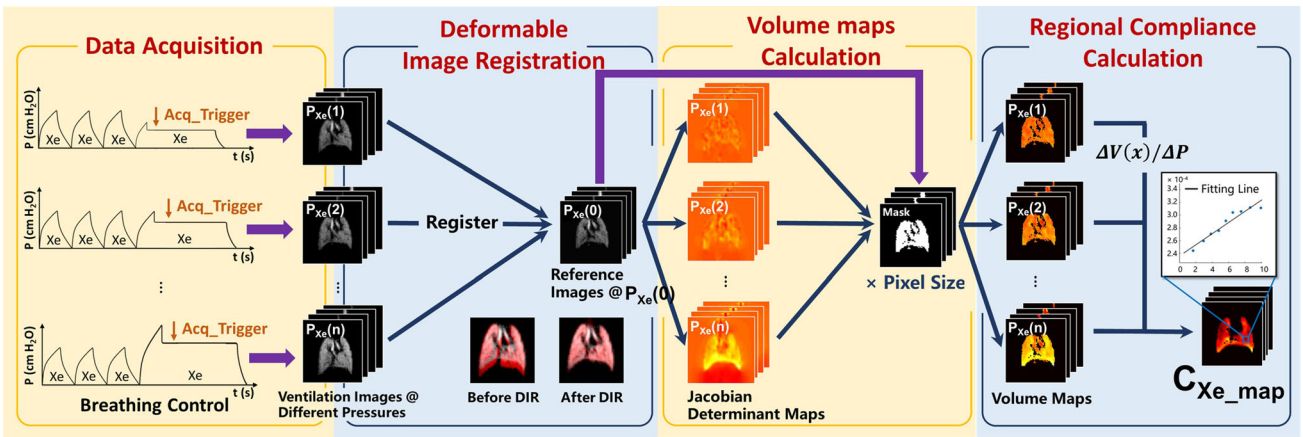

FIGURE 1: The schematic for data acquisition and lung compliance maps measurement using hyperpolarized ^{129}Xe MRI. After three xenon flushes, ventilation imaging was triggered during the breath-hold of the fourth xenon inhalation. The airway pressures were recorded in real-time by the LabView-controlled ventilator. For each rat, Advanced Normalization Toolkits (ANTs) was used to obtain the Jacobian determinant maps by registering the ventilation images with different breath-hold airway pressures ($P_{Xe}(1)$, …, $P_{Xe}(n)$) to the images with minimal pressure ($P_{Xe}(0)$). The image mismatch between images with pressures of $P_{Xe}(0)$ and $P_{Xe}(n)$ was obvious before DIR, and significantly reduced after DIR. Then, the volume maps with different pressures could be obtained by multiplying the Jacobian determinant maps by image masks with $P_{Xe}(0)$ and voxel size. Finally, after removing the trachea manually, C_{Xe} maps could be obtained voxel-by-voxel by fitting volume maps with different pressures to (1). C_{Xe_map} = regional lung compliance measured with hyperpolarized ^{129}Xe MRI; DIR = deformable image registration.

$$\mathrm{Vol}(\mathrm{P_{Xe}}(i),x) = J\left(\Psi_{\mathrm{Xe-P}(i)},x\right)\cdot \mathrm{Vol}(\mathrm{P_{Xe}}(0),x), i = 1,\ldots,\mathrm{n}, \quad (2)$$

where $\mathrm{Vol}(\mathrm{P_{Xe}}(i), x)$ and $J(\Psi_{\mathrm{Xe\text{-}P}(i)}, x)$ are the voxel volume and Jacobian determinant at position x in the ^{129}Xe images that correspond to pressure $\mathrm{P_{Xe}}(i)$, respectively, and $\mathrm{Vol}(\mathrm{P_{Xe}}(0), x)$ is the voxel size, which is determined by the image spatial resolution. The 3D distribution of lung compliance was calculated by linearly fitting all volume maps and corresponding airway pressures voxel-by-voxel using the following equation:

$$\Delta\mathrm{Vol_{Xe}}(i,x) = \mathrm{C_{Xe\_map}}(x)\cdot\Delta\mathrm{P_{Xe}}(i),\ i = 1,\ldots,\mathrm{n}, \quad (3)$$

$$\Delta\mathrm{Vol_{Xe}}(i,x) = \mathrm{Vol}(\mathrm{P_{Xe}}(i),x) - \mathrm{Vol}(\mathrm{P_{Xe}}(0),x);$$
$$\Delta\mathrm{P_{Xe}}(i) = \mathrm{P_{Xe}}(i) - \mathrm{P_{Xe}}(0),$$

where $\mathrm{C_{Xe\_map}}(x)$ is the lung compliance at position x in the ^{129}Xe image at pressure $\mathrm{P_{Xe}}(0)$.

Global and regional lung compliance based on CT images were also calculated. Lung region segmentation was performed using CT-Analyser software (Bruker, Billerica, MA, USA), and global and regional lung compliance measured with CT (i.e, $\mathrm{C_{CT}}$ and $\mathrm{C_{CT\_map}}$) were calculated using a similar process to that used for the calculation of $\mathrm{C_{Xe}}$ and $\mathrm{C_{Xe\_map}}$. The detailed description can be found in the Supplementary Data 2.

For both $\mathrm{C_{Xe\_map}}$ and $\mathrm{C_{CT\_map}}$, the R-squared (R^2) for the P-V curve-fitting was also obtained for each voxel. Before further analysis, the trachea was removed from the lung compliance maps. The repeatability of $\mathrm{C_{Xe}}$ and $\mathrm{C_{Xe\_map}}$ calculation was demonstrated in four naive rats, as shown in Table S1 and Fig. S2 in the Supplemental Material.

Direction-Dependencies Analysis

Direction-dependencies of lung compliance were also analyzed based on the derived $\mathrm{C_{Xe\_map}}$ and $\mathrm{C_{CT\_map}}$. In particular, the 3D regional lung compliance was divided into six regions along the apical-basal (A-B), anterior-posterior (A-P), and right-left (R-L) directions. Apical-basal, anterior-posterior, and right-left lung were segmented using the geometrical center of the lung (i.e., the center slice from the apex to base, the center slice from ventral to dorsal lung, and the bifurcation of the trachea, respectively). Regional lung compliance ratios were calculated for A-B, A-P, and R-L directions, denoted as $\mathrm{R_{A\text{-}B}}$, $\mathrm{R_{A\text{-}P}}$, and $\mathrm{R_{R\text{-}L}}$, respectively. For example, $\mathrm{R_{A\text{-}B}}$ was calculated as $\mathrm{C_B/C_A}$, where $\mathrm{C_B}$ and $\mathrm{C_A}$ represented the mean regional lung compliance in basal and apical regions, respectively. Moreover, $\mathrm{R_{A\text{-}P}}$ and $\mathrm{R_{R\text{-}L}}$ were calculated in the same manner.

Quantitative Histology

The rats were euthanized after CT examination, and the lungs were extracted immediately. The extracted lungs were filled with 4% paraformaldehyde solution (Biosharp, Hefei, Anhui, China) at an airway pressure of 25 cm H_2O for more than 2 hours and then kept in the same solution for more than 48 hours. Thereafter, the lungs were embedded in paraffin, cut into 5-μm-thick tissue sections, and stained with hematoxylin and eosin (H&E, Hycell, Wuhan, Hubei, China). For each section, images without large airway were acquired using a microscope (Nikon Eclipse Ts 100; Nikon Corp., Tokyo, Japan).[21,26] A standard test grid was overlaid on the images, and the septal wall thickness was determined as the average of total truncated length.[27] All sections for each rat were used to calculate the alveolar septal wall thickness automatically using a home-built Matlab script (version 2021a; The MathWorks Inc., Natick, MA, USA).

Statistical Analysis

All statistical analyses were performed using SPSS (version 18; IBM Corp., Armonk, NY, USA). Data were first tested for normality using the Shapiro–Wilk test, see Table S2 in the Supplemental Material. Results were presented as mean ± SD and median and interquartile range for normal and non-normal distributed data, respectively. Unpaired *t*-tests and Mann–Whitney *U* tests were used to compare parameters obtained from PFTs, ^{129}Xe MRI, CT, and quantitative histology between the control and fibrosis groups. Pearson correlation coefficients (r) were used to determine the relationship between the obtained physiological parameters (i.e., $\mathrm{C_{Xe}}$, $\mathrm{C_{Xe\_map}}$, $\mathrm{C_{CT}}$, $\mathrm{C_{CT\_map}}$, $\mathrm{C_{qs}}$, and FVC) and the septal wall thickness. Paired *t*-tests and Wilcoxon signed-rank test were used for comparing lung compliance in each direction to assess the direction-dependencies of lung compliance. A P-value <0.05 was considered statistically significant.

Results

Pulmonary Function Tests and Histological Analysis

The measured $\mathrm{C_{qs}}$, IC, FVC, and TLC were lower in the fibrosis group than in the control group: 0.48 ± 0.12 mL/cm H_2O, 4.73 ± 1.11 mL, 6.46 ± 1.34 mL, and 8.48 ± 1.84 mL for the fibrosis group, respectively, and 0.89 ± 0.08 mL/cm H_2O, 7.87 ± 1.21 mL, 10.19 ± 0.86 mL, and 10.90 ± 1.85 mL for the fibrosis group, respectively (Table 1; $P < 0.01$). In the histological section, clear alveolar wall thickening was observed for the fibrosis case (Fig. S3 in the Supplemental Material). The septal wall thickness in the fibrosis group was higher than that in the control group (control: 5.99 ± 0.55 μm, fibrosis: 10.12 ± 2.95 μm, $P = 0.002$).

Global Lung Compliance Measured With Xenon MRI and Chest CT

On ^{129}Xe MRI and CT images, visible lung inflation was observed in the control rat, whereas there was minimal inflation in the fibrosis rat with similar airway pressure differences (Fig. 2a). The airway pressure is recorded throughout the experiment, and the data during the breath-hold are averaged. The variance of pressure within a single breath-hold is less than 0.5 cm H_2O, while the difference in airway pressure between adjacent imaging is >1 cm H_2O. P-V curves derived from ^{129}Xe MRI and chest CT showed lower change of lung volume in the fibrosis rat than the control rat, wherein $\mathrm{C_{Xe}}$ was 0.28 vs. 0.54 (mL/cm H_2O), respectively (Fig. 2b), and $\mathrm{C_{CT}}$ was 0.22 vs. 0.41 (mL/cm H_2O), respectively (Fig. 2c). The global lung compliance measurements $\mathrm{C_{Xe}}$ and $\mathrm{C_{CT}}$ were

TABLE 1. Basic Information, Pulmonary Function Tests, and Quantitative Histological Results

Variable	Control	Fibrosis	*P*-Value
N	10	10	-
Age[a] (wk)	9	9	-
Weight[a] (g)	269 ± 12 (260, 278)	253 ± 29 (232, 273)	0.125
IC (mL)	7.87 ± 1.21 (7.00, 8.73)	4.73 ± 1.11 (3.93, 5.52)	<0.001[b]
FVC (mL)	10.19 ± 0.86 (9.57, 10.81)	6.46 ± 1.34 (5.50, 7.42)	<0.001[b]
FEV_{100} (mL)	3.44 ± 0.51 (3.07, 3.80)	3.52 ± 0.60 (3.09, 3.95)	0.747
TLC (mL)	10.90 ± 1.85 (9.57, 12.22)	8.48 ± 1.84 (7.17, 9.79)	0.009[b]
C_{qs} (mL/cm H_2O)	0.89 ± 0.08 (0.83, 0.94)	0.48 ± 0.12 (0.40, 0.57)	<0.001[b]
Septal wall thickness (μm)	5.99 ± 0.55 (5.59, 6.38)	10.12 ± 2.95 (8.01, 12.23)	0.002[b]

Data are presented as mean ± SD and 95% confidence interval. IC = inspiratory capacity; FVC = forced vital capacity; FEV_{100} = forced expiratory volume in 100 msec; TLC = total lung capacity; C_{qs} = quasi-static lung compliance.
[a]Age and weight are the data during the experiment.
[b]Unpaired *t*-test, $P < 0.05$.

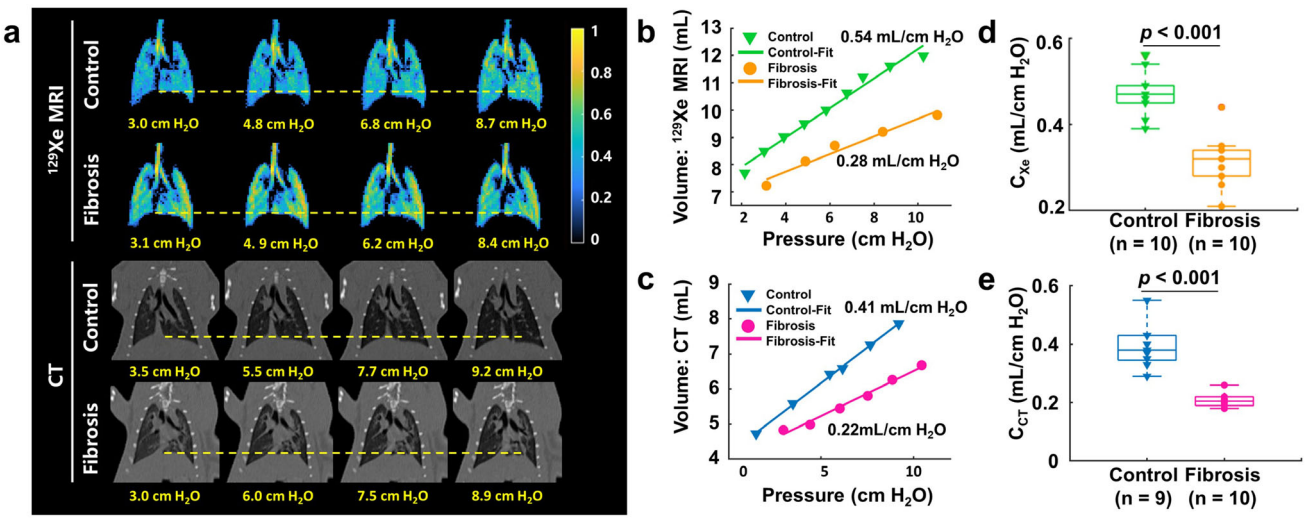

FIGURE 2: Lung imaging and global lung compliance measurement with ^{129}Xe MRI and computed tomography (CT). (a) ^{129}Xe ventilation images and chest CT images of typical control and fibrosis rats, the dotted lines indicate the diaphragmatic surface location in the minimal pressure images. In similar airway pressure changes (^{129}Xe MRI: 5.7 cm H_2O for the control rat vs. 5.3 cm H_2O for the fibrosis rat, chest CT: 5.7 cm H_2O for the control rat vs. 5.9 cm H_2O for the fibrosis rat), visible lung inflation was observed in the control rat but not in the fibrosis rat. (b) Typical pressure-volume (P-V) curves derived from ventilation images. (c) Box plots of global static lung compliance measured with hyperpolarized ^{129}Xe MRI (C_{Xe}). (d) Typical P-V curves derived from segmented CT lung images. (e) Box plots of global static lung compliance measured with CT (C_{CT}). CT = computed tomography.

lower in the fibrosis group than the control group: C_{Xe} was 0.31 ± 0.06 vs. 0.47 ± 0.05 (mL/cm H_2O) ($P < 0.001$), respectively (Fig. 2d), and C_{CT} was 0.21 ± 0.03 vs. 0.39 ± 0.07 (mL/cm H_2O) ($P < 0.001$), respectively (Fig. 2e).

Regional Lung Compliance Measurement

Higher lung compliance was observed in the basal areas compared to the apical areas in the control rat in both ^{129}Xe MRI and CT lung compliance maps (Fig. 3a): the mean of C_{Xe_map} was 0.47 (0.41, 0.56) vs. 0.37 (0.32, 0.39) [$\times 10^{-4}$ mL/cm H_2O], respectively ($P = 0.005$), and the mean of C_{CT_map} was 0.58 ± 0.12 vs. 0.38 ± 0.05 [$\times 10^{-6}$ mL/cm H_2O], respectively ($P < 0.001$). Such differences were attenuated in the basal and apical areas of fibrosis rat: the mean of C_{Xe_map} was 0.24 (0.21, 0.32) vs. 0.22 (0.19, 0.29) [$\times 10^{-4}$ mL/cm H_2O], respectively ($P = 0.009$), and the mean of C_{CT_map} was 0.43 ± 0.10 vs. 0.31 ± 0.07

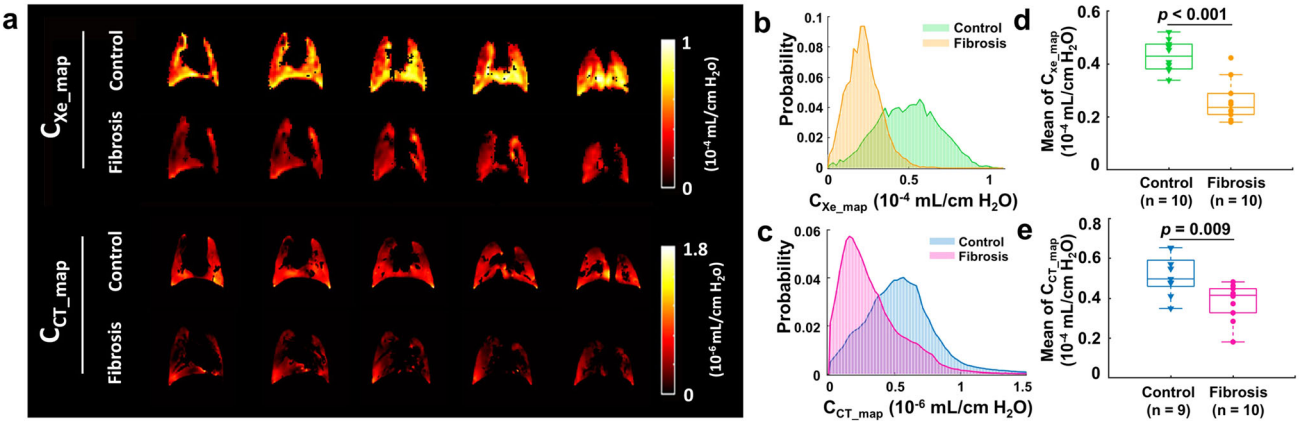

FIGURE 3: Regional lung compliance analysis. (a) Typical C_{Xe_map} and C_{CT_map} from the control and fibrosis groups. Compared to the apical areas, higher lung compliance was observed in basal areas in the control group. (b, c) The histogram of C_{Xe_map} and C_{CT_map} of the representative rats from both groups, respectively. The y-axis represents the proportion of the number of voxels within a certain value range to the total number of voxels in the entire lung compliance map. (d, e) Box plots of mean of C_{Xe_map} and C_{CT_map} from control and fibrosis groups, respectively. C_{Xe_map} and C_{CT_map} = regional lung compliance measured with hyperpolarized ^{129}Xe MRI and chest CT, respectively. CT = computed tomography.

[$\times 10^{-6}$ mL/cm H_2O], respectively ($P < 0.001$). In the lung compliance measured with ^{129}Xe MRI, lower lung compliance values are more frequently observed in the fibrosis rat when compared to these in the control rat, resulting in a right-skewed histogram distribution (Fig. 3b): the kurtosis was 3.04 ± 0.46 vs. 5.39 ± 2.41 ($P = 0.013$), respectively; the skewness was 0.37 ± 0.20 vs. 0.99 ± 0.50 ($P = 0.003$), respectively. Although similar distribution of lung compliance values with chest CT are observed in a typical rat (Fig. 3c), no differences in kurtosis and skewness were found between the control and fibrosis groups: the kurtosis was 5.23 ± 0.77 vs. 5.51 ± 1.21 ($P = 0.557$), respectively; the skewness was 1.04 ± 0.15 vs. 1.17 ± 0.34 ($P = 0.316$), respectively. The mean of C_{Xe_map} was lower in fibrosis group than controls (0.26 ± 0.08 vs. 0.43 ± 0.06 [$\times 10^{-4}$ mL/cm H_2O], respectively, $P < 0.001$; Fig. 3d), and the mean of C_{CT_map} was lower in fibrosis group than controls (0.38 ± 0.09 vs. 0.52 ± 0.10 [$\times 10^{-6}$ mL/cm H_2O], respectively, $P = 0.009$; Fig. 3e). For C_{Xe_map}, the R^2 were different between the two groups (control: 0.86 [0.84, 0.87], fibrosis: 0.77 [0.69. 0.81], $P = 0.001$). However, no difference was observed for R^2 measurements between two groups in the measured C_{CT_map} (control: 0.81 ± 0.09, fibrosis: 0.81 ± 0.08; $P = 0.916$). Moreover, despite the different derivation processes, C_{Xe} was strongly correlated with the sum of C_{Xe_map} (Fig. S4 in the Supplemental Material).

Direction-Dependencies Assessment of Lung Compliance

The whole lung was segmented into six regions across three directions (Fig. 4a). Both C_{Xe_map} and C_{CT_map} were higher ($P < 0.05$) in the control group than in the fibrosis group for all six regions (Fig. 4b,c), and the results were summarized in Table 2. In controls, higher ^{129}Xe lung compliance was observed in the basal vs. the apical regions (0.47 [0.41, 0.56] vs. 0.37 [0.32, 0.39] [$\times 10^{-4}$ mL/cm H_2O], $P = 0.005$), posterior vs. the anterior regions (0.44 [0.39, 0.52] vs. 0.40 [0.36, 0.45] [$\times 10^{-4}$ mL/cm H_2O], $P = 0.005$), and left vs. the right lung (0.46 ± 0.07 vs. 0.41 ± 0.05 [$\times 10^{-4}$ mL/cm H_2O], $P < 0.001$). Moreover, in controls, higher CT lung compliance was observed in the basal vs. and apical regions (0.58 ± 0.12 vs. 0.38 ± 0.05 [$\times 10^{-6}$ mL/cm H_2O], $P < 0.001$), anterior vs. posterior regions for the control group (0.54 ± 0.08 vs. 0.49 ± 0.09 [$\times 10^{-6}$ mL/cm H_2O], $P = 0.009$). However, difference was observed only between the apical and basal regions for the fibrosis group in both C_{Xe_map} (0.22 [0.19, 0.29] vs. 0.24 [0.21, 0.32] [$\times 10^{-4}$ mL/cm H_2O], $P = 0.009$) and C_{CT_map} (0.31 ± 0.07 vs. 0.43 ± 0.10 [$\times 10^{-6}$ mL/cm H_2O], $P < 0.001$) (Table 2). Additionally, higher $R_{A\text{-}B}$ was observed in the control group than the fibrosis group for ^{129}Xe MRI (1.35 ± 0.13 vs. 1.12 ± 0.09, $P < 0.001$; Fig. 5a), and higher $R_{A\text{-}P}$ was observed in the fibrosis group than the control group for chest CT (1.02 [0.93, 1.06] vs. 0.91 [0.84, 0.96], $P = 0.041$; Fig. 5b). The ellipsoidal visualization well depicts the changes in R in three directions from C_{Xe_map} and C_{CT_map} between the groups (Fig. 5c,d).

Correlation of the Image-Derived Lung Compliance, PFTs, and Quantitative Histology

Figure 6 depicts the correlation of C_{Xe}, mean of C_{Xe_map}, C_{CT}, and mean of C_{CT_map} with C_{qs}, and FVC measured with PFTs, and the septal wall thickness measured with quantitative histology, respectively. C_{Xe} correlated with C_{qs} ($r = 0.891$), FVC ($r = 0.851$), and septal wall thickness ($r = -0.709$). Similarly, the mean of C_{Xe_map} correlated with C_{qs} ($r = 0.873$), FVC ($r = 0.771$), and septal wall thickness ($r = -0.773$). For lung compliance derived from chest CT,

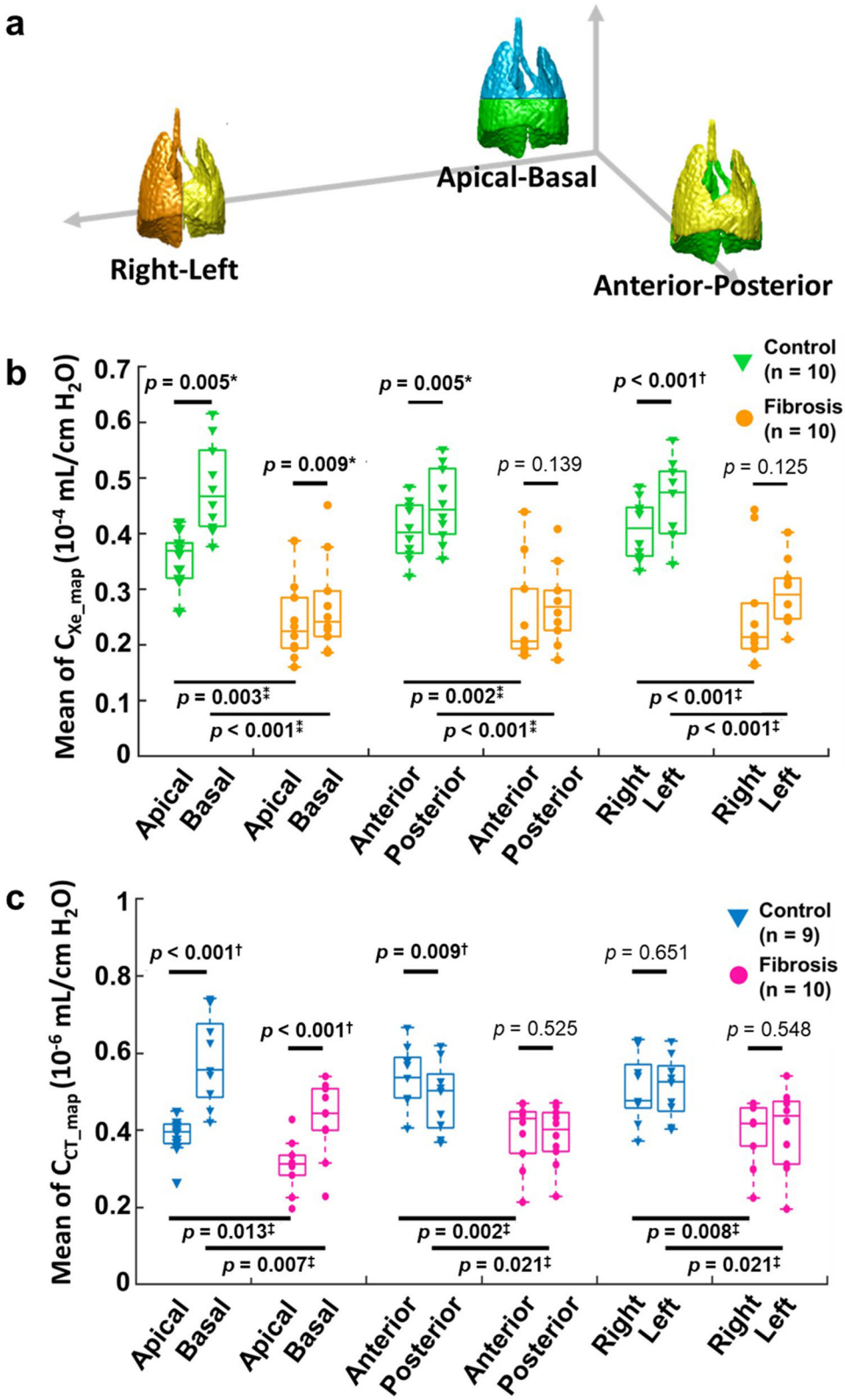

FIGURE 4: Comparison of lung compliance in different regions. (**a**) Schematic of lung segmentation in three directions and six regions for following quantitative analysis. (**b**, **c**) Boxplots of C_{Xe_map} and C_{CT_map}, respectively. The mean of C_{Xe_map} and C_{CT_map} in each region of the fibrosis group was significantly lower than that of the control group (bottom bar in [b] and [c]). Moreover, significant differences were observed in the three directions in C_{Xe_map} of the control group (top bar in [b]), and were observed in apical-basal and anterior-posterior direction in C_{CT_map} of the control group (top bar in [c]). C_{Xe_map} and C_{CT_map} = regional lung compliance measured with hyperpolarized ^{129}Xe MRI and chest CT, respectively; † denotes paired *t*-test, $P < 0.05$; ‡ denotes unpaired *t*-test, $P < 0.05$; * denotes Wilcoxon signed-rank test, $P < 0.05$; ⁑ denotes Mann–Whitney *U* test, $P < 0.05$. CT = computed tomography.

TABLE 2. The Mean of the Regional Lung Compliance Measured With Hyperpolarized ^{129}Xe MRI (C_{Xe_map}) and Chest CT (C_{CT_map}) in Different Regions of the Lung

	^{129}Xe MRI			Chest CT		
	Control	Fibrosis	*P*-Value*	Control	Fibrosis	*P*-Value*
N	10	10	-	9	10	-
Apical-Basal						
Apical	0.37 (0.32, 0.39)	0.22 (0.19, 0.29)	0.003[a]	0.38 ± 0.05 (0.34, 0.42)	0.31 ± 0.07 (0.25, 0.35)	0.013[b]
Basal	0.47 (0.41, 0.56)	0.24 (0.21, 0.32)	<0.001[a]	0.58 ± 0.12 (0.49, 0.67)	0.43 ± 0.10 (0.35, 0.51)	0.007[b]
P-value**	0.005[c]	0.009[c]	-	<0.001[d]	<0.001[d]	-
Anterior-Posterior						
Anterior	0.40 (0.36, 0.45)	0.21 (0.19, 0.32)	0.002[a]	0.54 ± 0.08 (0.47, 0.60)	0.39 ± 0.08 (0.32, 0.45)	0.002[b]
Posterior	0.44 (0.39, 0.52)	0.27 (0.22, 0.31)	<0.001[a]	0.49 ± 0.09 (0.42, 0.56)	0.39 ± 0.08 (0.32, 0.45)	0.021[b]
P-value**	0.005[c]	0.139	-	0.009[d]	0.525	-
Right-Left						
Right	0.41 ± 0.05 (0.37, 0.45)	0.25 ± 0.10 (0.18, 0.33)	<0.001[b]	0.51 ± 0.09 (0.45, 0.57)	0.39 ± 0.08 (0.31, 0.49)	0.008[b]
Left	0.46 ± 0.07 (0.41, 0.51)	0.29 ± 0.06 (0.25, 0.33)	<0.001[b]	0.51 ± 0.08 (0.44, 0.58)	0.40 ± 0.11 (0.32, 0.45)	0.021[b]
P-value**	<0.001[d]	0.125	-	0.651	0.548	-

Results were presented as mean ± SD and 95% confidence interval, and median and interquartile range of the voxel in the whole region for normal and non-normal distributed data, respectively. The unit of lung compliance: ^{129}Xe MRI: 10^{-4} mL/cm H_2O; CT: 10^{-6} mL/cm H_2O. CT = computed tomography.
[a]Mann–Whitney *U* test, $P < 0.05$.
[b]Unpaired *t*-test, $P < 0.05$.
[c]Wilcoxon signed-rank test, $P < 0.05$.
[d]Paired *t*-test, $P < 0.05$.
*The *P*-value is comparison between the control and fibrosis group.
**The *P*-value is comparison for different regions.

C_{CT} correlated with C_{qs} ($r = 0.794$), FVC ($r = 0.509$), and septal wall thickness ($r = -0.582$). However, the mean of C_{CT_map} only correlated with C_{qs} ($r = 0.548$).

Discussion

In this study, we proposed an approach for quantifying lung compliance globally and regionally using hyperpolarized ^{129}Xe MRI. For a dataset of 20 rats with and without pulmonary fibrosis, we observed reduced static lung compliance in the pulmonary fibrosis group compared with the control group. The ^{129}Xe MRI-derived lung compliance was correlated with that measured using PFTs. In addition, we performed comprehensive experiments to investigate regional lung compliance in the A-B, A-P, and R-L directions.

We observed lower lung compliance in the fibrosis group compared to the control group using both hyperpolarized ^{129}Xe MRI and PFTs. The lower lung compliance measured with PFTs in the fibrosis group is in agreement with that previously reported in a pulmonary fibrosis model induced by bleomycin.[28] This result most likely relates to septal and intra-alveolar fibrosis caused by the intratracheal instillation of bleomycin, which can induce expansion of the myofibroblast population and increased deposition of extracellular matrix.[20] These changes were also confirmed by histology and PFTs. The thickening of the alveolar wall could

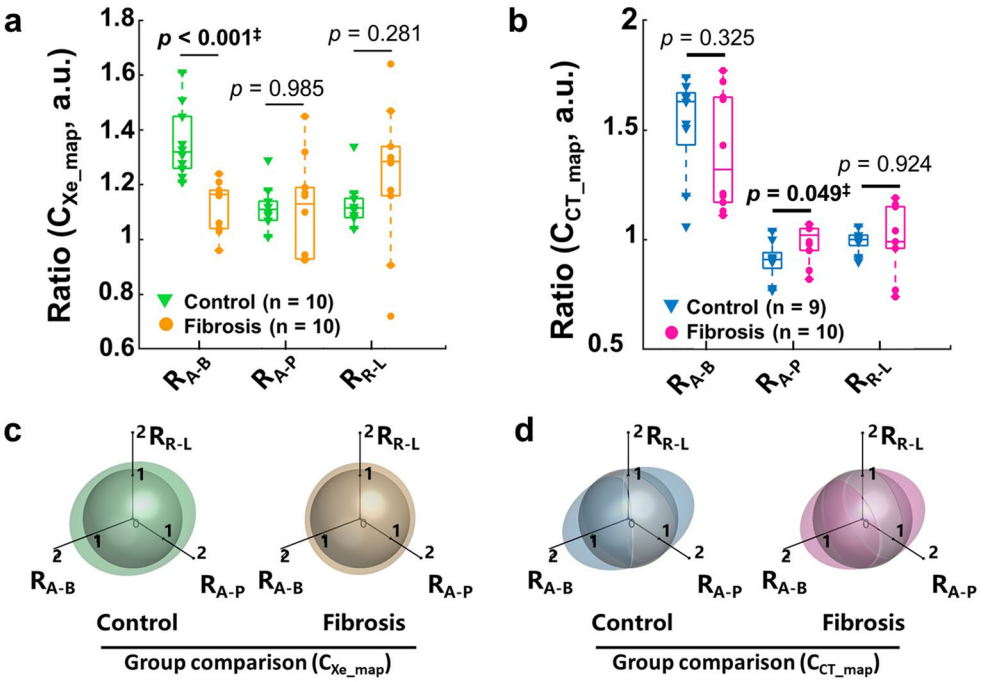

FIGURE 5: Direction-dependencies analysis of lung compliance. (a, b) Box plots of regional lung compliance ratios (R_{A-B}, R_{A-P}, and R_{R-L}) measured with ^{129}Xe MRI and CT, respectively. A significant difference was observed in R_{A-B} with ^{129}Xe MRI between the groups, and was observed in R_{A-P} with CT between the groups. (c, d) Visual assessments of R_{A-B}, R_{A-P}, and R_{R-L} using ^{129}Xe MRI and CT, respectively. The gray unit sphere was shown as a reference. The R_{A-B} with ^{129}Xe MRI was significantly longer than 1 in the control group and close to 1 in the fibrosis group, whereas the R_{A-P} with CT was significantly lower than 1 in the control group and close to 1 in the fibrosis group. A-B = apical-basal; A-P = anterior-posterior; R-L = right-left. ‡ Denotes unpaired *t*-test, $P < 0.05$. CT = computed tomography.

be observed in the fibrosis group, and IC, FVC, and TLC were different between the two groups. These observations are in agreement with those reported in previous studies.[28,29]

Global static lung compliance measured with hyperpolarized ^{129}Xe MRI (C_{Xe}) was lower than that obtained with PFTs. This may be mainly caused by lung hysteresis, which can result in inconsistencies between the inspiratory and expiratory P-V curves.[30,31] Furthermore, C_{qs} was measured during exhalation,[32] whereas C_{Xe} was measured during inhalation,[17] whereby higher pressure is needed to inflate the lung. Previous studies also reported that lung volume at any given pressure during deflation was greater than that during inflation,[31,33] and that lung compliance measured during expiration was higher than that measured during inspiration at low airway pressure.[5] Nevertheless, our result showed that C_{Xe} had a strong correlation with C_{qs}. In addition, C_{Xe} was also strongly correlated with FVC, which is usually used as a surrogate endpoint of IPF in clinical settings.[2] The correlation between C_{Xe} and FVC suggests that hyperpolarized ^{129}Xe MRI-based lung compliance can be used as a potential imaging biomarker of lung mechanics for pulmonary fibrosis evaluation.

The lung compliance calculation may be affected by errors in the measurement of lung volume and airway pressure. For lung volume measurement, the loss of xenon signals mainly stems from T_1 decay induced by residual paramagnetic oxygen and gas exchange between alveolar structures and capillaries. In our study, T_1 decay was minimized by three xenon flushes, and gas exchange-related signal loss was ignored because the signal of dissolved-phased xenon was only about 2% of the gas phase xenon.[34] Airway pressure is expected to decrease slightly during breath-hold due to the resolution of inhale pressure gradients and potential imperfect tracheal seal. During ventilation imaging, a typical standard deviation of the recorded airway pressure was less than 0.5 cm H_2O, which was lower than the pressure increment between adjacent ventilation imaging (typically 1 to 2 cm H_2O). To minimize the influences of airway pressure and ensure accurate lung compliance measurement, we acquired ^{129}Xe MRI data at multiple pressure points and limited the airway breath-hold pressure to 0–10 cm H_2O, which was also used when measuring the C_{qs} in PFTs. The upper limit of airway pressure was set at 10 cm H_2O because the elastic elements of the lung would exceed the limit of the distensibility when the pressure is higher than 10 cm H_2O,[30] which may result in incorrectly lower lung compliance measurements.

In addition to the global evaluation, we also quantified the regional distribution of lung compliance. The goodness-of-fit R^2 of C_{Xe_map} in the control group was higher than that in the fibrosis group. The lower R^2 in the fibrosis group

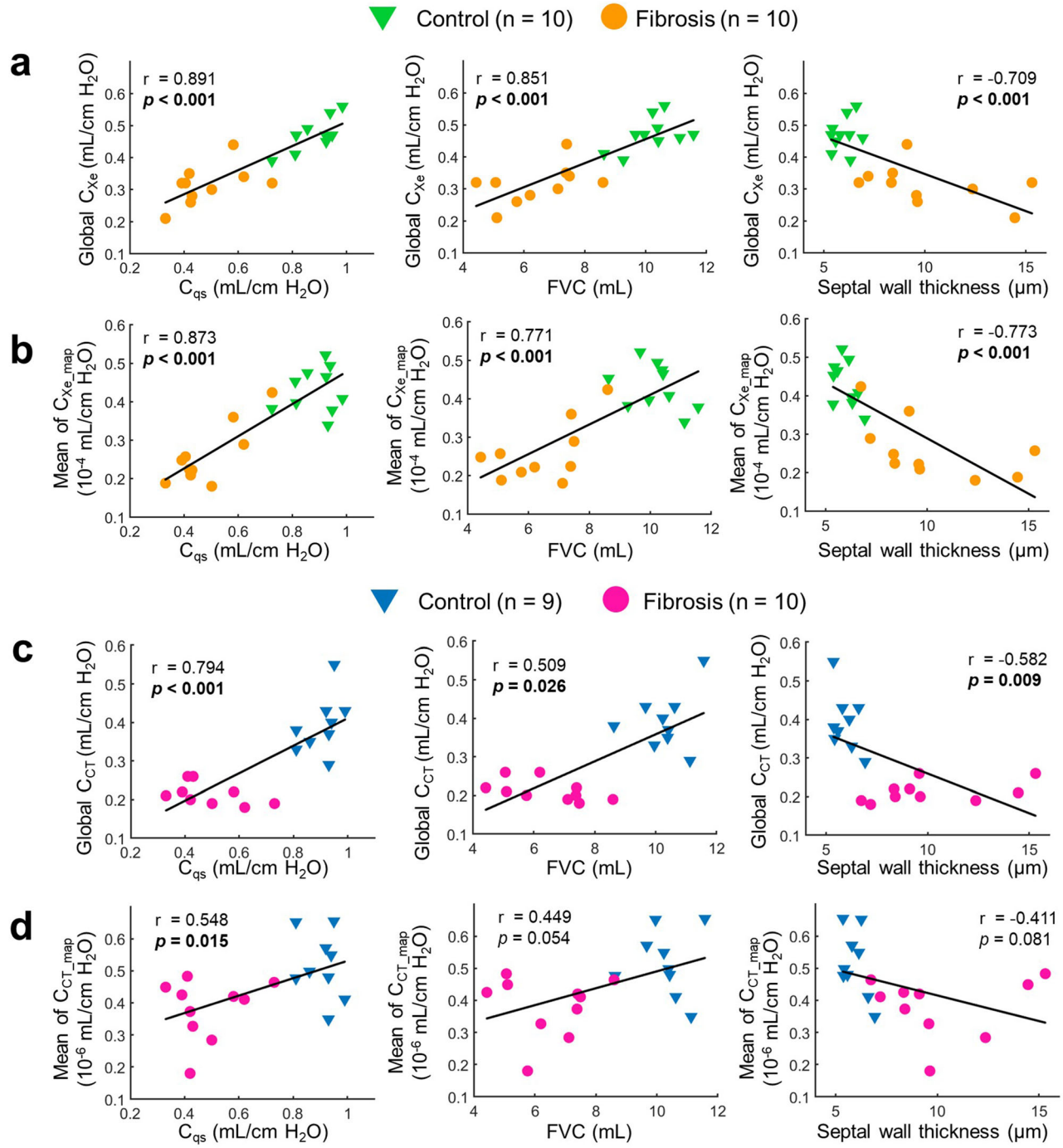

FIGURE 6: Correlation of image-derived lung compliance with PFTs and quantitative histology. (a–d) Correlation of C_{Xe}, mean of C_{Xe_map}, C_{CT}, and mean of C_{CT_map} with C_{qs}, FVC, and septal wall thickness, respectively. C_{Xe} and C_{CT} = global static lung compliance measured with hyperpolarized ^{129}Xe MRI and chest CT, respectively; C_{Xe_map} and C_{CT_map} = regional lung compliance measured with hyperpolarized ^{129}Xe MRI and chest CT, respectively; C_{qs} = quasi-static lung compliance; FVC = forced vital capacity; PFTs = pulmonary function tests; CT = computed tomography.

might be caused by the difficulties in lung expansion and the low signal-to-noise ratio (SNR) in the lesion areas, which may lead to nonlinearity of the P-V curve and errors in the Jacobian determinant maps via image registration, respectively. Nevertheless, the R^2 for both groups exceeded 0.7, suggesting good fitting. Both C_{Xe} and the mean of C_{Xe_map} showed strong correlations with C_{qs} and FVC, suggesting potential of hyperpolarized ^{129}Xe MRI-derived lung compliance for early diagnosis of pulmonary fibrosis. Although the lung volumes in C_{Xe} and C_{Xe_map} were computed using different approaches, both metrics were self-consistent.

We observed higher lung compliance in basal and posterior regions than that in apical and anterior regions in the control group. The higher lung compliance in the basal

region was probably related to anatomical conditions as the basal lung is far from the sternum. Also, greater motion near the diaphragm would presumably contribute to higher lung compliance in the lung bases. For the posterior region, a previous study has shown that the supine position was associated with greater motion in the posterior part of the diaphragm,[35] which means the posterior region would expand more easily during inspiration, resulting in higher compliance. Additionally, higher compliance was observed in the left lung vs. the right lung, which may be attributed to the anatomy of rat lungs. In rats, the right and left lung have four and one lobes, respectively, and less bifurcations would make the left lung inflate more easily. In the fibrosis group, we observed that the direction-dependencies in lung compliance were reduced in the A-B direction and disappeared in the A-P and R-L directions, compared to the control group. These results indicate the difficulties in lung inflation caused by fibrosis, which is associated with increased pulmonary rigidity and the fibrous thickening of alveolar septa, leading to shortness of breath.[36]

Lung compliance measured with ^{129}Xe MRI and CT was also compared in this study. Both global lung compliance measured with MRI (i.e., C_{Xe}) and chest CT (i.e., C_{CT}) were higher in the controls compared with the fibrosis group. The measured C_{CT} in our study is in agreement with that reported previously.[37] Although both C_{Xe} and C_{CT} are calculated based on image-derived volumes, they differ intrinsically in lung volume calculation. In CT images, the measured lung volumes represent the thoracic volume, which contains the lung tissue. However, the measured lung volume with ^{129}Xe images represents the gas volume within the ventilated area of the lung. For the measurement of lung compliance based on the gas volume changes during inspiration and expiration, lung compliance measured with ^{129}Xe gas MRI would theoretically be more accurate.

For the regional lung compliance, the mean of C_{Xe_map} is two orders of magnitude higher that of C_{CT_map}. This can be attributed to the different spatial resolution between the two imaging modalities. When calculating C_{Xe_map} and C_{CT_map}, the change in lung volume for each voxel is based on the voxel volume from images with minimal pressure. The voxel volume of ^{129}Xe gas MRI was 100-fold that of chest CT, such a difference is consistent with the difference between the means of C_{Xe_map} and C_{CT_map}. Moreover, lung compliance measured with ^{129}Xe MRI (C_{Xe} and C_{Xe_map}) showed strong correlation with C_{qs}, FVC, and septal wall thickness. However, the correlations between C_{CT} and FVC, C_{CT} and septal wall thickness are weaker, and C_{CT_map} only has a correlation with C_{qs}. These results suggest that lung compliance measured with hyperpolarized gas MRI may be more accurate than lung compliance measured with CT.

Limitations

Despite the good statistical significance in our study, the sample size in our study is relatively small, and larger sample size is needed in the following studies to obtain more reliable statistical results. Then, we used the airway pressure for global and regional lung compliance calculation, but it may not accurately represent the heterogeneous transpulmonary pressure distribution across the lung. Previous study has performed regional transpulmonary pressure measurement in animal models and human cadavers using pleural sensors and esophageal balloons,[38] and precise measurement of local lung pressure should be considered in future studies. Moreover, lung segmentation from the ^{129}Xe images was used for regional lung compliance analysis. However, this procedure could be optimized by incorporating CT or proton MRI data to analyze lung compliance of each lung lobe. In addition, the establishment of a theoretical model is also necessary for investigating the relationships between lung compliance measured using hyperpolarized ^{129}Xe imaging and pulmonary physiological parameters, such as alveolar elasticity and the degree of fibrosis. Last but not least, although bleomycin-induced pulmonary fibrosis is the best-characterized murine model in use today,[20] the data from IPF patients remains essential to apply the proposed method to the real clinical setting and to understand the distribution characteristics of lung compliance in pulmonary fibrosis. These limitations also represent our future research directions.

Conclusion

In this study, we proposed an approach for quantifying both global and regional lung compliance in a rat model with pulmonary fibrosis using hyperpolarized xenon gas MRI. With the proposed approach, regional lung compliance changes were readily evaluated, and direction-dependencies were also obtained.

Acknowledgments

The authors wish to thank Dr. Cheng Wang and Dr. Luyang Shen for useful discussion on ^{129}Xe image registration during the data processing. This work was supported by National Key Research and Development Program of China (2022YFC2410000 and 2018YFA0704000), National Natural Science Foundation of China (82127802, 21921004, 82372150, 81930049, and 82202119), the Strategic Priority Research Program of the Chinese Academy of Sciences (XDB0540000), Key Research Program of Frontier Sciences, CAS (ZDBS-LY-JSC004), Hubei Provincial Key Technology Foundation of China (2021ACA013), Major Program (JD) of Hubei Province (2023BAA021), and Hubei Provincial Outstanding Youth Fund (2023AFA112). Haidong Li and Xiuchao Zhao acknowledge the support from Youth Innovation Promotion Association, CAS (2020330 and 2021330).

References

1. Todd NW, Luzina IG, Atamas SP. Molecular and cellular mechanisms of pulmonary fibrosis. Fibrogenesis Tissue Repair 2012;5:1-24.
2. Raghu G, Collard HR, Egan JJ, et al. An official ATS/ERS/JRS/ALAT statement: Idiopathic pulmonary fibrosis: Evidence-based guidelines for diagnosis and management. Am J Respir Crit Care Med 2011;183: 788-824.
3. Plantier L, Cazes A, Dinh-Xuan A-T, Bancal C, Marchand-Adam S, Crestani B. Physiology of the lung in idiopathic pulmonary fibrosis. Eur Respir Rev 2018;27:170062.
4. Soroksky A, Esquinas A. Goal-directed mechanical ventilation: Are we aiming at the right goals? A proposal for an alternative approach aiming at optimal lung compliance, guided by esophageal pressure in acute respiratory failure. Crit Care Res Pract 2012;2012:1-9.
5. Nair GB, Al-Katib S, Podolsky R, Quinn T, Stevens C, Castillo E. Dynamic lung compliance imaging from 4DCT-derived volume change estimation. Phys Med Biol 2021;66:21NT06.
6. Guerrero T, Castillo R, Sanders K, Price R, Komaki R, Cody D. Novel method to calculate pulmonary compliance images in rodents from computed tomography acquired at constant pressures. Phys Med Biol 2006;51:1101-1112.
7. Jang GY, Ayoub G, Kim YE, et al. Integrated EIT system for functional lung ventilation imaging. Biomed Eng Online 2019;18:83.
8. Chitturi V, Farrukh N. Spatial resolution in electrical impedance tomography: A topical review. J Electr Bioimpedance 2017;8:66-78.
9. Haas M, Hamm B, Niehues SM. Automated lung volumetry from routine thoracic CT scans: How reliable is the result? Acad Radiol 2014;21: 633-638.
10. Li H, Zhao X, Wang Y, et al. Damaged lung gas exchange function of discharged COVID-19 patients detected by hyperpolarized ^{129}Xe MRI. Sci Adv 2021;7:eabc8180.
11. Stewart NJ, Norquay G, Griffiths PD, Wild JM. Feasibility of human lung ventilation imaging using highly polarized naturally abundant xenon and optimized three-dimensional steady-state free precession. Magn Reson Med 2015;74(2):346-352.
12. Xiao S, Deng H, Duan C, et al. Highly and adaptively undersampling pattern for pulmonary hyperpolarized ^{129}Xe dynamic MRI. IEEE Trans Med Imaging 2018;38:1240-1250.
13. Wang JM, Robertson SH, Wang ZY, et al. Using hyperpolarized Xe-129 MRI to quantify regional gas transfer in idiopathic pulmonary fibrosis. Thorax 2018;73:21-28.
14. Hajari AJ, Yablonskiy DA, Sukstanskii AL, Quirk JD, Conradi MS, Woods JC. Morphometric changes in the human pulmonary acinus during inflation. J Appl Physiol 2012;112:937-943.
15. Marshall H, Collier GJ, Johns CS, et al. Imaging collateral ventilation in patients with advanced chronic obstructive pulmonary disease: Relative sensitivity of ^{3}He and ^{129}Xe MRI. J Magn Reson Imaging 2019;49:1195-1197.
16. Driehuys B, Martinez-Jimenez S, Cleveland ZI, et al. Chronic obstructive pulmonary disease: Safety and tolerability of hyperpolarized ^{129}Xe MR imaging in healthy volunteers and patients. Radiology 2012;262(1): 279-289.
17. Fox MS, Ouriadov A, Santyr GE. Comparison of hyperpolarized ^{3}He and ^{129}Xe MRI for the measurement of absolute ventilated lung volume in rats. Magn Reson Med 2014;71:1130-1136.
18. Choy S, Wheatley A, McCormack DG, Parraga G. Hyperpolarized ^{3}He magnetic resonance imaging-derived pulmonary pressure-volume curves. J Appl Physiol 2010;109:574-585.
19. Stephen MJ, Emami K, Woodburn JM, et al. Quantitative assessment of lung ventilation and microstructure in an animal model of idiopathic pulmonary fibrosis using hyperpolarized gas MRI. Acad Radiol 2010;17: 1433-1443.
20. Moore BB, Hogaboam CM. Murine models of pulmonary fibrosis. Am J Physiol Lung Cell Mol Physiol 2008;294:L152-L160.
21. Zhang M, Li H, Li H, et al. Quantitative evaluation of lung injury caused by $PM_{2.5}$ using hyperpolarized gas magnetic resonance. Magn Reson Med 2020;84:569-578.
22. Nouls J, Fanarjian M, Hedlund L, Driehuys B. A constant-volume ventilator and gas recapture system for hyperpolarized gas MRI of mouse and rat lungs. Concept Magn Reson B 2011;39:78-88.
23. Ridler T, Calvard S. Picture thresholding using an iterative selection method. IEEE Trans Syst Man Cybern 1978;8:630-632.
24. Shekhar R, Lei P, Castro-Pareja CR, Plishker WL, D'Souza WD. Automatic segmentation of phase-correlated CT scans through nonrigid image registration using geometrically regularized free-form deformation. Med Phys 2007;34:3054-3066.
25. Avants BB, Tustison N, Song G. Advanced normalization tools (ANTS). Insight J 2009;2:1-35.
26. Li H, Zhang Z, Zhao X, Sun X, Ye C, Zhou X. Quantitative evaluation of radiation-induced lung injury with hyperpolarized xenon magnetic resonance. Magn Reson Med 2016;76:408-416.
27. Woods JC, Choong CK, Yablonskiy DA, et al. Hyperpolarized ^{3}He diffusion MRI and histology in pulmonary emphysema. Magn Reson Med 2006;56:1293-1300.
28. Braun RK, Broytman O, Braun FM, et al. Chronic intermittent hypoxia worsens bleomycin-induced lung fibrosis in rats. Respir Physiol Neurobiol 2018;256:97-108.
29. Yu X, Zhang Y, Yang X, et al. The influence of BuqiHuoxueTongluo formula on histopathology and pulmonary function test in bleomycin-induced idiopathic pulmonary fibrosis in rats. Evid Based Complement Alternat Med 2018;2018:1-13.
30. Shofer S, Badea C, Qi Y, Potts E, Foster WM, Johnson GA. A micro-CT analysis of murine lung recruitment in bleomycin-induced lung injury. J Appl Physiol 2008;105:669-677.
31. Schmitt J-M, Vieillard-Baron A, Augarde R, Prin S, Page B, Jardin F. Positive end-expiratory pressure titration in acute respiratory distress syndrome patients: Impact on right ventricular outflow impedance evaluated by pulmonary artery Doppler flow velocity measurements. Crit Care Med 2001;29:1154-1158.
32. Frazer D, Lindsley W, McKinney W, et al. A model of the recruitment-derecruitment and volume of lung units in an excised lung as it is inflated-deflated between minimum and maximum lung volume. J Biomech Eng 2013;135:034503.
33. Cheng W, DeLong D, Franz G, Petsonk E, Frazer D. Contribution of opening and closing of lung units to lung hysteresis. Respir Physiol 1995;102:205-215.
34. Marshall H, Stewart NJ, Chan H-F, Rao M, Norquay G, Wild JM. In vivo methods and applications of xenon-129 magnetic resonance. Prog Nucl Mag Rer Sp 2021;122:42-62.
35. Takazakura R, Takahashi M, Nitta N, Murata K. Diaphragmatic motion in the sitting and supine positions: Healthy subject study using a vertically open magnetic resonance system. J Magn Reson Imaging 2004; 19:605-609.
36. Mandal S, Balas VE, Shaw RN, Ghosh A. Prediction analysis of idiopathic pulmonary fibrosis progression from OSIC dataset. *2020 IEEE International conference on computing, power and communication technologies (GUCON). Greater Noida*: IEEE; 2020. p 861-865.
37. Siddiqui S, Xin Y, Profka H, Kadlecek S, Rizi RR. Using microct to quantify the compliance of lungs in a bleomycin-induced pulmonary fibrosis rat model. American Thoracic Society 2016 International Conference. San Francisco; 2016:A5008.
38. Yoshida T, Amato MB, Grieco DL, et al. Esophageal manometry and regional transpulmonary pressure in lung injury. Am J Respir Crit Care Med 2018;197:1018-1026.